FH AACHEN
UNIVERSITY OF APPLIED SCIENCES

FACHHOCHSCHULE AACHEN (FH)
CAMPUS JÜLICH
UNIVERSITY OF APPLIED SCIENCES

The Faculty of Energy Technology
Physical Engineering

The elastic properties of $MnFe_4Si_3$ and Mn_4FeSi_3 measured with Resonant Ultrasound Spectroscopy

By

Yue Qiu

Bachelor thesis

October 2014

Prepared at

Jülich Centre for Neutron Science JCNS-2

Peter Grünberg Institut PGI, JARA-FIT,

Forschungszentrum Jülich GmbH

JÜLICH
FORSCHUNGSZENTRUM

Jülich Centre for Neutron Science

Referee 1: **Prof. Dr. rer. nat. Arnold Förster / FH Aachen**

Referee 2: **Dr. Karen Friese / Forschungszentrum Jülich**

Supervisor: **Herlitschke Marcus / Forschungszentrum Jülich**

I hereby confirm that this bachelor thesis was completed entirely by myself. No other sources or literature reference than the ones mentioned.

Date Signature

Acknowledgement

I am heartily grateful to Prof. Dr. rer. nat. Arnold Förster and Dr. Karen Friese being my referee for this bachelor thesis. I would like to express my sincere thanks to Herlitschke Marcus being my supervisor and giving me the guidance and advice during this work and for the thesis. I also want to sincerely thank Hering Paul and Persson Joerg to help and guide me.

It is my pleasure to thank Prof. Dr. Th. Brückel offering me the opportunity to work on this thesis at Jülich Centre for Neutron Science JCNS and Peter Grünberg Institut PGI, JARA-FIT, Forschungszentrum Jülich GmbH, JCNS-2.

Finally, thanks all members of JCNS-2 giving me a god work environmental and helping during this work.

Table of Contents

1. Introduction

Solving the problem of environmental pollution is an ongoing task for research, nowadays. Two approaches are possible, either more ecologically friendly processes of energy production must be supported or the current produced energy must be more efficiently used. One possibility for energy saving is based on the magnetic refrigeration process at room-temperature, which was reported to exhibit a potential energy saving of 20%-30% [1]. This process is based on the magnetocaloric effect (MCE), which the temperature change of a material triggered by the application or removal of a magnetic field. The individual members of the series $Mn_{5-x}Fe_xSi_3$ (x=0-5) are known for their magnetocaloric properties [2]. The magnetic phase transitions and the magnetocaloric properties of the individual compounds have been studied by magnetization measurements. Although the MCE in these materials is only of moderate size, they are still good candidates for further optimization via e.g. doping as they are composed of cheap and non-toxic elements. Furthermore, it is possible to synthesize these materials as large single crystals, which is not possible for most other magnetocaloric materials (MCM). This is a major advantage for investigating the fundamental mechanism of the magnetocaloric effect as a series of experimental techniques are only viable if large single crystals are available.

This manuscript reports the characterization of the elastic properties of selected compounds in the $Mn_{5-x}Fe_xSi_3$ series. The method of choice to obtain the elastic properties is investigated by Resonant Ultrasound Spectroscopy (RUS). This method allows quantifying the elastic properties by measuring their characteristic resonance spectra. The advantage of RUS compared to other methods is that it is possible to determine the complete elastic tensor of a material out of one single measurement. However, obtaining all elastic moduli requires single crystals, since in a polycrystalline material only two of the elastic moduli can be characterized [3]. Thus, to be able to characterize the full elastic moduli of the compounds, large single crystal of individual compounds in the $Mn_{5-x}Fe_xSi_3$ series were synthesized in the course of this thesis using the Czochralski method.

The investigations presented here are focused on two compounds in the series, Mn_4FeSi_3 (x=1) and $MnFe_4Si_3$ (x=4) due to time limitations. These two representatives are the most interesting ones, since the compound with x=4 has the magnetocaloric transition at room-

temperature and is thus a promising candidate for applications and the compound *x*=1, which has the magnetocaloric transition below 100K, has exactly the reverse iron to manganese ratio [2]. The combination of the studies on both compounds is thus promising for studying the effect of exchange of Mn for Fe on the elastic properties.

In the following, the elastic moduli of $MnFe_4Si_3$ were presented for different magnetic fields at room temperature in order to observe the influence of the magnetic field on the magnetic transitions. For the Mn_4FeSi_3 sample investigation were carried out at different temperatures and in different fields. The obtained resonance frequencies are given as a function of temperatures and magnetic fields and furthermore, elastic properties are extracted from these data at various temperatures.

2. Theory

2.1 Elasticity of solid

Materials will deform when a force is applied to them, and, in case the material is elastic, it will return to its original shape after the force is removed. The elastic moduli describe an object's tendency to be deformed elastically under load. They are defined as the proportional constants between any strain in a solid (strain is displacement caused by applying a stress) and the corresponding stress (the stress is the force per unit area). This stress-strain relationship can be adequately described by Hooke's law. However, all real solids dissipate energy when strained and are not elastic for large deformations, thus Hook's law is not strictly valid. Therefore elastic moduli are useful only in case of low dissipation. The general form of Hook's law is

$$\sigma_{ij} = c\varepsilon_{ij}$$

Where σ is the stress tensor, c is the stiffness tensor and ε is the resulting strain tensor. Subscript i refer to the direction of applied stress and j refer to the direction of the resulting strain. If $i=j$, the deformation is assumed to be compressional. If not, the deformation is a shear process.

In the general 3-D case, the stress and the strain tensor are 2nd rank tensors with 9 stress components σ_{ij} (3 compressional, 6 shear) as shown in Figure 2.1 and 9 strain components ε_{kl}, respectively.

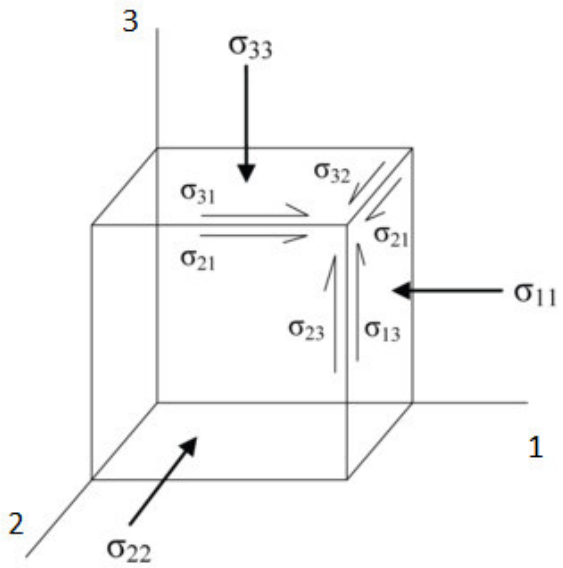

Figure 2.1: For a 3-D object, an off-axis surface stress produces nine stress components [4].

The stiffness tensor c_{ijkl} is a tensor of fourth order, i.e., it is represented by a 9×9 matrix. However, due to the fact that σ_{ij} and ε_{kl} are symmetric tensors (for example $\sigma_{12}=\sigma_{21}$, $\varepsilon_{13}=\varepsilon_{31}$), some components are similar or related to each other and thus the 9×9 matrix can be reduced to a 6×6 matrix through the following translation of subscripts [3]:

11→1, 22→2, 33→3

23(or 32) →4, 13(or 31) →5, 12(or 21) →6

Using this notation the new matrix represents a crystal with 21 independent elastic moduli. Therefore, the general form of the Hooke's law is given by

$$\begin{pmatrix}\sigma_1\\ \sigma_2\\ \sigma_3\\ \sigma_4\\ \sigma_5\\ \sigma_6\end{pmatrix} = \begin{pmatrix}c_{11} & c_{12} & c_{13} & c_{14} & c_{15} & c_{16}\\ c_{21} & c_{22} & c_{23} & c_{24} & c_{25} & c_{26}\\ c_{31} & c_{32} & c_{33} & c_{34} & c_{35} & c_{36}\\ c_{41} & c_{42} & c_{43} & c_{44} & c_{45} & c_{46}\\ c_{51} & c_{52} & c_{53} & c_{54} & c_{55} & c_{56}\\ c_{61} & c_{62} & c_{63} & c_{64} & c_{65} & c_{66}\end{pmatrix}\begin{pmatrix}\varepsilon_1\\ \varepsilon_2\\ \varepsilon_3\\ \varepsilon_4\\ \varepsilon_5\\ \varepsilon_6\end{pmatrix}$$

Nevertheless, the symmetry of the crystal can force some of the elastic moduli to be identical or can require them to be zero. Thus in high symmetrical crystals, such as cubic or hexagonal, the number of elastic moduli can be significantly reduced. As an example, for a hexagonal structure, only 5 independent elastic moduli and one additional elastic modulus

c_{66} that is calculated from $\frac{c_{11}-c_{12}}{2}$ are needed to describe the elasticity of solid. The form of the elastic matrix is then:

$$\begin{pmatrix} c_{11} & c_{12} & c_{13} & 0 & 0 & 0 \\ c_{12} & c_{11} & c_{13} & 0 & 0 & 0 \\ c_{13} & c_{13} & c_{33} & 0 & 0 & 0 \\ 0 & 0 & 0 & c_{44} & 0 & 0 \\ 0 & 0 & 0 & 0 & c_{44} & 0 \\ 0 & 0 & 0 & 0 & 0 & c_{66} \end{pmatrix}$$

2.2 Sound propagation in elastic material

Within a material, the atoms (or ions, molecules) perform vibrational motions about their equilibrium positions. If a material is not stressed or compressed beyond its elastic limit, the individual particles perform elastic oscillations. When the particles are displaced from their equilibrium positions, the restoring forces will arise from the resistance of the solid itself. The constants describing the resistance to deformation are called elastic moduli (see section 2.1) [5]. If one considers the connection of particles as elastic springs as shown in Figure 2.2, all the particles have an influence on neighboring particles.

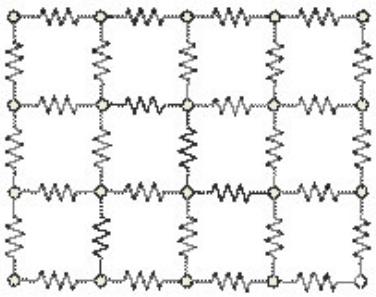

Figure 2.2: Oscillating masses or particles connected by means of elastic springs [6].

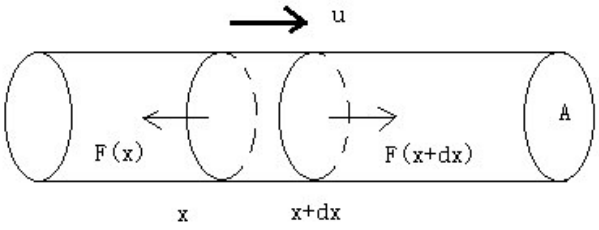

Figure 2.3: A long rod is used as a simple system to illustrate the effect of sound wave on the atoms in the material. The drawing is inspired by [3].

Sound waves travel with different speed in different materials, since the mass of atomic particles and the spring constants are different. Consider the following simple system which is shown in Figure 2.3. In a long rod with cross-section area *A* and density *ρ*, a longitudinal wave of compression leads to a displacement *u* of a particular atom in the rod from its equilibrium position. According to Newton's second law

$$(\rho A dx)\frac{d^2u}{dt^2} = F(x+dx) - F(x)$$

and

$$\rho\frac{d^2u}{dt^2} = \frac{1}{A}\frac{dF}{dx} = \frac{d\sigma_{ij}}{dx}$$

where σ_{ij} is the compression stress.

Hooke's law and the strain, defined as $\varepsilon = \frac{du}{dx}$, lead to the equation for a long rod with propagating longitudinal waves (i.e. waves that move the atoms parallel to the direction of travel of the wave).

$$\frac{d^2u}{dt^2} = \left(\frac{c_{ij}}{\rho}\right)\frac{d^2u}{dx^2}$$

This is solved by

$$u(x,t) = u_0 e^{i(kx-\omega t)}$$

Where

$$\frac{\omega}{k} = \sqrt{\frac{c_{ij}}{\rho}} = C_E$$

The above expression is a general equation for compressional waves to get the Young's modulus speed of sound C_E. The subscript i of Young's modulus *c* refers to the direction of applied stress and *j* refers to the direction of the resulting strain.

2.3 The resonance of a spring

An object vibrates after an initial stimulus with a driving force. The frequency of this vibration is called natural frequency. Every object has its own natural frequencies, depending on the material and the geometry of the object. If a periodically varying force is applied to the object, it vibrates with the same frequency as the applied force. This is called

forced vibration. If the frequency of the applied force coincides with the natural frequency of the material, the amplitude of vibration will reach a maximum value. This phenomenon is called resonance, and the corresponding frequency is called resonance frequency.

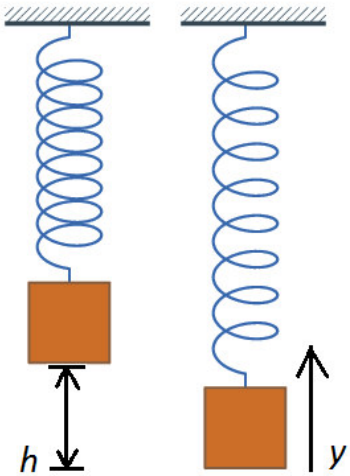

Figure 2.4: Model of a spring and a mass to illustrate the resonance frequency. The drawing is inspired by [7].

In order to calculate exemplary a resonant vibrational frequency, a model system of a spring and a mass is given, as shown as Figure 2.4. The spring is stretched the distance h by the attached mass. Hooke's law (neglecting damping and the mass of the spring) leads to:

$$F = -kh$$

Where, k is spring constant. Using Newton's second law, one obtains the equation of motion:

$$mg - kx = ma = m\frac{d^2y}{dt^2}$$

Where, m is the mass attached to the spring and g is the acceleration due to gravity. This differential equation can be solved with the ansatz

$$y = A\sin(\omega t - \varphi)$$

Where

A is the amplitude of motion, ω is the angular frequency, φ is a phase constant. This ansatz is applied to the differential equation and solved for ω. The expression for the resonant vibrational frequency is thus given by:

$$\omega^2 = \frac{k}{m}$$

$$f = \frac{1}{2\pi}\sqrt{\frac{k}{m}}$$

2.4 Crystal growth

Crystallization is defined as a phase change within a crystalline product growing from solution (or from a gas phase). Crystallization from a solution can be thought of as a two steps process. The first step is nucleation that is the creation of small nuclei containing the newly formed crystals. Nucleation refers to the beginning of the phase separation process. Nucleation occurs relatively slow as the initial components of the future crystals must impinge on each other in the correct orientation and placement to form the crystal. When the solution is saturated and encounters a dust particle or a solid surface, for example, a seed crystal will tend to adsorb and aggregate on the surface. The solid surface thus provides the nucleation site for the formation of crystals [8]. Nuclei that succeed in achieving the critical cluster size will then start growing in a second step. New atoms, ions, molecules or polymers will be added to the nucleus and will be arranged into the lattices.

A solution which is used for crystallization must be supersaturated. Supersaturated solution means the solution contains more atoms than under saturation. Supersaturation is needed as the driving force. Otherwise nucleation and growth cannot occur continuously and simultaneously. Depending on the individual conditions, the process of nucleation and growth can lead to crystals with different sizes and shapes.

The structure of the crystal surface is the basis of the crystal growth theories. The Kossel model of the crystal surface is the most common model in use and shown in Figure 2.5. In this model, the crystal surface is described as consisting of cubic units. Edge vacancies and

kinks appear along the steps of the surface. The area between the steps is called a terrace. The terraces may contain both ad-atoms (the growth units attached to the surface) and terrace surface vacancies. In this model, ad-atoms will form one bond and atoms attached to the steps and kinks will form two and three bonds, respectively. Hence, kink sites will offer the most stable configuration and further ad-atoms will be incorporated preferentially close to the location of the kink until they reach the face edge. Then a new layer can be formed by the above procedure. Therefore, mechanisms of growth can be represented as Figure 2.6.

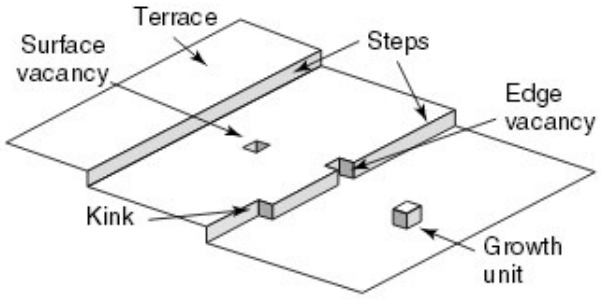

Figure 2.5: Kossel model of a crystal surface [9].

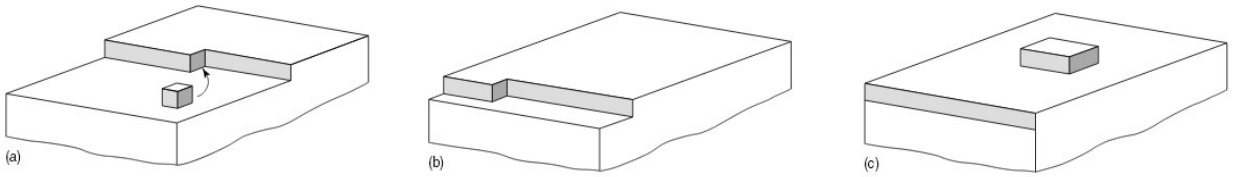

Figure 2.6: Schematic representation of crystal growth. a) Incorporation of growth units to kink. b) The step is formed close to the face edge. c) Formation of nucleus [9].

2.5 Single-crystal X-ray diffraction

Single-crystal X-ray diffraction is a non-destructive analytical technique that provides the basis for the determination of the crystal structure of the material. Crystals are solids characterized by an ordered, periodic arrangement of atoms (ions, molecules).

The basic unit of a crystal structure is called unit cell. If one combines the unit cell with translations in the three directions of space, a crystal is generated. Each crystal structure is characterized by its symmetry and crystallizes in one of the 230 space groups. Thus a single crystal is a perfect periodic arrangement of atoms, with a periodically repeating crystal lattice. In Figure 2.7, sketches of crystalline, polycrystalline, and amorphous states are depicted. Comparing with single crystal, a polycrystal contains various orientation and size of small single crystals. An amorphous material has random arrangement of atoms, for example, glass is a common amorphous material.

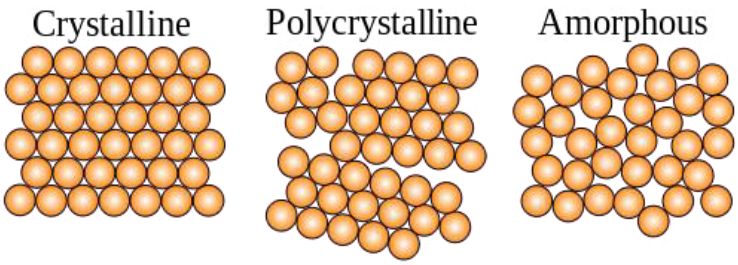

Figure 2.7: Schematic representation of the crystalline, polycrystalline, and amorphous state [10].

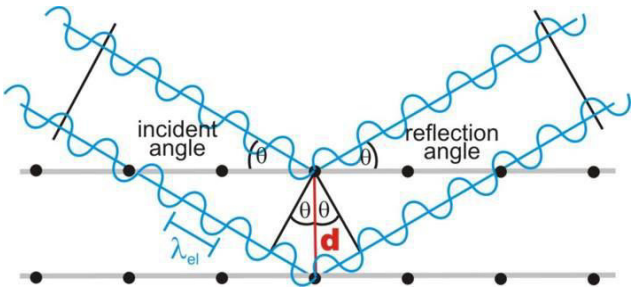

Figure 2.8: Two waves incident in the spacing of crystal with distance *d* of lattice [11].

As X-rays have wavelengths that are comparable to typical distances within a crystal lattice, they provide an effective method to analyze the crystal structure. X-rays are generated in a cathode ray tube, in which a tungsten filament is heated by a generator which applies a current. The filament emits electrons that accelerate towards a target metal. Upon striking the target, the electrons have energy to dislodge inner shell electrons of the target material, the X-rays are generated.

X-rays propagate as waves. If two waves which propagate close to each other meet, constructive interference between them can only occur if they have the same wavelength and are in phase. Sir William H. Bragg and Sir W. Lawrence Bragg described the condition for constructive interference of waves scattered by the periodic arrangement of atoms in a crystal. This is illustrated in Figure 2.8. Incoming waves of wavelength λ are scattered by two parallel lattices planes with an interspacing d under an incident angle θ. To obtain constructive interference, the path difference between the two incident and the scattered waves, which is $2d \sin\theta$, has to be an integer of wavelength λ of the incident X-ray, so that

$$2d \sin\theta = n\lambda$$

This expression is known as Bragg's law.

2.6 Magnetism and magnetic phase transition

The magnetic moments of atoms can, depending on temperature and applied magnetic field, align in different ordered states. The disordered paramagnetic state and selected ordering schemes are sketched in Figure 2.9. In the paramagnetic state the magnetic spins are randomly arranged. This state is present in all magnetic materials above their magnetic order temperature. The ferromagnetic state is defined by spontaneous ordering of the spins in the same direction, even without applied magnetic field. In case the spins are aligned anti-parallel to each other and the overall sum of the magnetization is zero, one calls this anti-ferromagnetism. Ferrimagnetism is an anti-parallel alignment, in which the magnetic moments do not compensate each other completely.

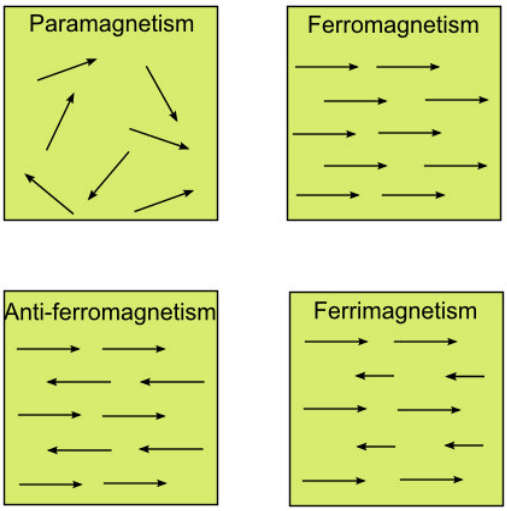

Figure 2.9: Four different types of magnetic states are sketched: paramagnetism, ferromagnetism, anti-ferromagnetism and ferrimagnetism.

The transition between disordered and ordered arrays of atomic magnetic moments or the transition between two differently ordered states is called magnetic transition. If the ordered phase has a net spontaneous magnetization below ordering temperature, the Curie-Weiss law can be used to describe the degree of magnetization. The degree of magnetization is called magnetic susceptibility x and is given by:

$$x = \frac{M}{H} = \frac{C}{T - T_c}$$

M is the magnetization (magnetic moment per unit volume), H is magnetic field, C is the material-specific Curie constant and T_c is the ordering temperature, also known as Curie temperature. If the magnetic material transforms from paramagnetism to ferromagnetism at a critical temperature, this temperature is called the Néel temperature.

2.7 The Magnetocaloric effect

The magnetocaloric effect (MCE) is defined as the temperature change of a magnetic material by the application or removal of a magnetic field. Magnetic refrigeration is a cooling technique based on the MCE. The magnetocaloric material (MCM) is separated into two subsystems in a typical magnetic refrigeration cycle: the magnetic moments and the lattice

[12]. The four main stages of the magnetic refrigeration cycle are illustrated in figure 2.10. In the absence of a magnetic field the orientations of the magnetic moments are in a random condition that is the material is in the paramagnetic state. With the application of the magnetic field the magnetic moments orient parallel to that field, decreasing the magnetic entropy. If the magnetization is performed in an adiabatic condition, the lattice entropy has to increase to compensate the decreasing magnetic entropy, as the overall entropy of the system stays constant. The increase in lattice entropy leads to an increase of the temperature of the material. The excessed heat can be removed through an exchange medium and the magnetic material is cooled back to the initial temperature. If then the magnetic field is removed, the magnetic entropy will rise again as the spins disorder. Again this is compensated by the lattice entropy which decreases leading to a decrease of the temperature of the material. This decrease in temperature can be used for cooling.

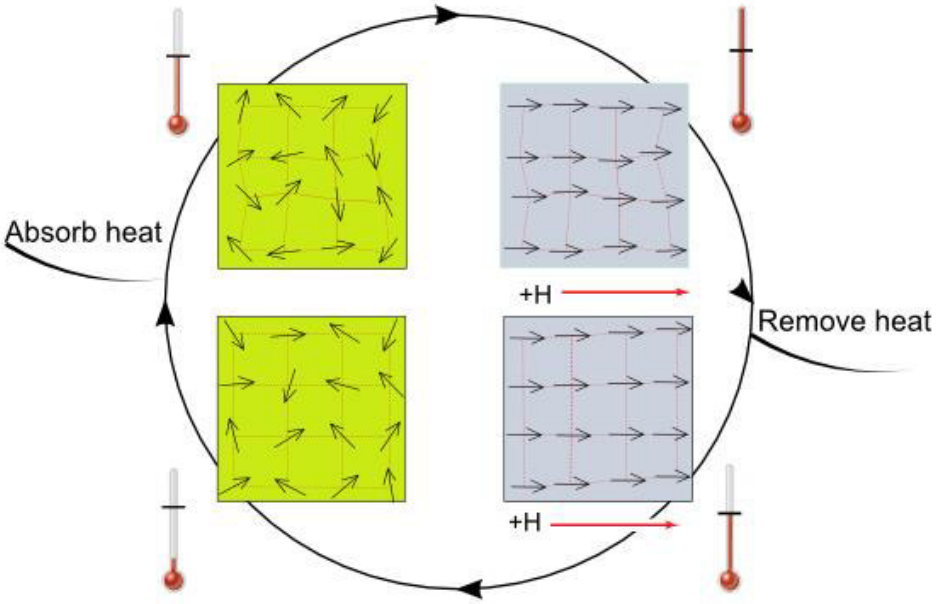

Figure 2.10: Illustration of a magnetic refrigeration cycle in four steps: a) Application of magnetic field leads to an increase of temperature. b) Removing of heat causes temperature reduction to the initial temperature. c) The removal of the magnetic field results in disordering of the spins and as a consequence a decrease of temperature below the initial temperature.

d) The temperature increases again by absorbing heat. The drawing is inspired by [13].

3. The Experimental Methods

3.1 Czochralski method

The Czochralski process [14] is a method of crystal growth used to obtain large single crystals. The process is commonly performed in an inert atmosphere. Figure 3.1 illustrates the setup for the growth of the single crystals used in this work by the Czochralski method.

The sample chamber is airtight and filled with argon. A seed crystal is mounted on a rod. Both of the seed crystal and the rod are made of tungsten. The holder is connected to an additional support unit made of aluminum oxide. A crucible of suitable size is put on the holder. Copper coils surround the holder. A generator supplies a large alternating current which passes through the coils to heat the solid which lies in the crucible. The solid is inductively heated due to its electrical conductivity. The seed crystal is immersed into the molten material and then slowly drawn out of the melt while the material will crystallize at the interface between the seed crystal and the melt. The precise control of the temperature gradients, the rate of pulling and the speed of rotation are key factors to obtain large single-crystals as cylindrical ingots from the melt.

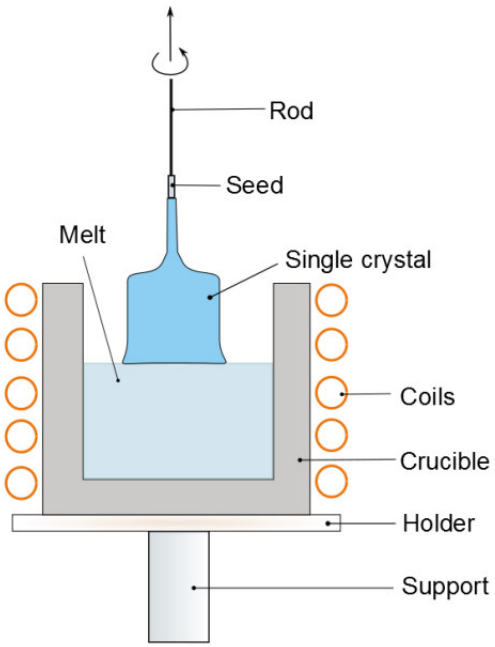

Figure 3.1: Illustration of the setup used for the growth of single crystals with the Czochralski method.

3.2 Laue method

The Laue Method [15] is a common method used to determine the orientation of large single crystals while white radiation is reflected from or transmitted through a fixed crystal. The incident angle θ is fixed in this method and each crystal plane (hkl) has a particular orientation with respect to the incoming beam. Consequently, only when the wavelength λ is satisfying Bragg's law (see section 2.5), constructive interference for the scattered beams from the set of parallel lattice planes can occur and a diffraction spot is recorded on the detector. Thus each spot corresponds to a set of parallel lattice planes (hkl) and a particular wavelength.

In the back-reflection method as shown in Figure 3.2 a), the film is placed between the x-ray source and the crystal. The beams, which are diffracted in a backward direction, are recorded on the detector. The Laue instrument used for our investigating was a Multiwire MWL100 Real-Time Back-Reflection Laue Camera System (MWL100 Camera System) and is displayed in Figure 3.2 b). It can be used for characterization and orientation of crystals by dynamically viewing the back-reflection images on a computer screen in real time. The grown crystal is fixed on a rotatable holder. The crystal is then rotated till a suitable orientation is found and a regular diffraction pattern is produced. The quality of the diffraction pattern directly allows judging the quality of the single crystal.

a) 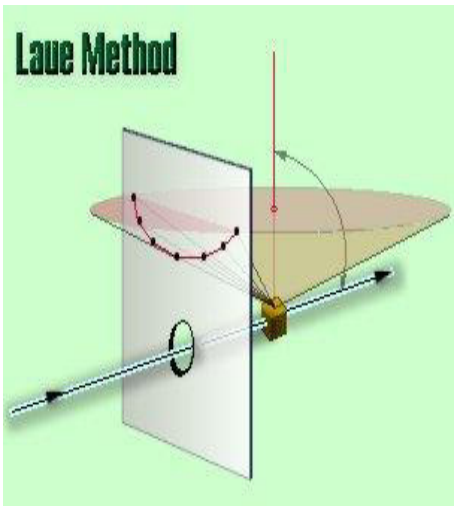

b) 

Figure 3.2: a) Illustration of the back- reflection method [16]. b) Multiwire MWL100 Real-Time Back-Reflection Laue Camera System (MWL100 Camera System) [17].

3.3 Traveling wire EDM

Electrical Discharge Machining (EDM) is an electrothermal cutting process. An illustration is shown in Figure 3.3. The piece of material that is being worked on is cut by a traveling cooper wire. Both the work piece and the wire are used as electrodes. A power supply is connected to the wire and work piece and produces electrical discharges (also called sparks) between them. The sparks then melt and vaporize parts of the work piece. The work piece is kept wet with deionized fluids as cooling fluid. The used deionized fluid then travels through a filter which removes the chips from the work piece.

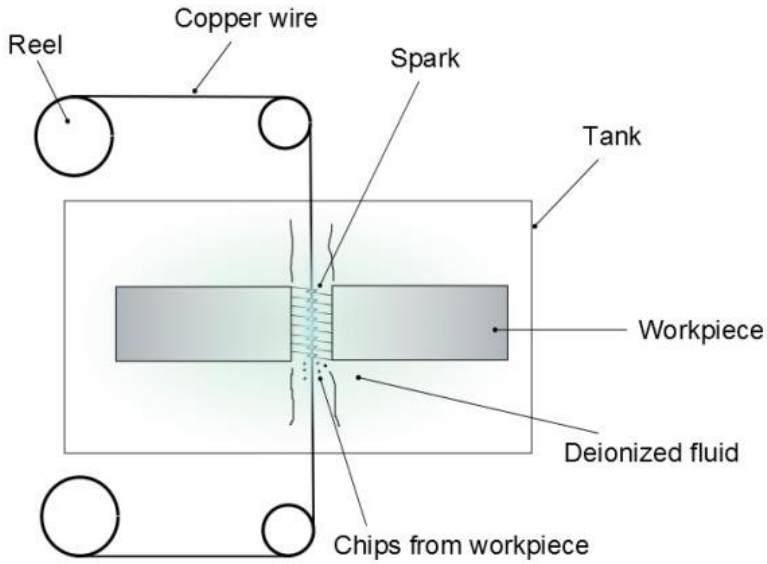

Figure 3.3: Illustration of traveling wire Electrical Discharge Machining. This draw is inspired by [18].

3.4 Resonant Ultrasound Spectroscopy

Resonant ultrasound spectroscopy is an experimental technique that allows quantifying the elastic properties of solids by measuring the acoustic resonance spectra. The advantage of RUS compared to other methods is that it is possible to determine the complete elastic tensor of a material out of one single measurement [19].

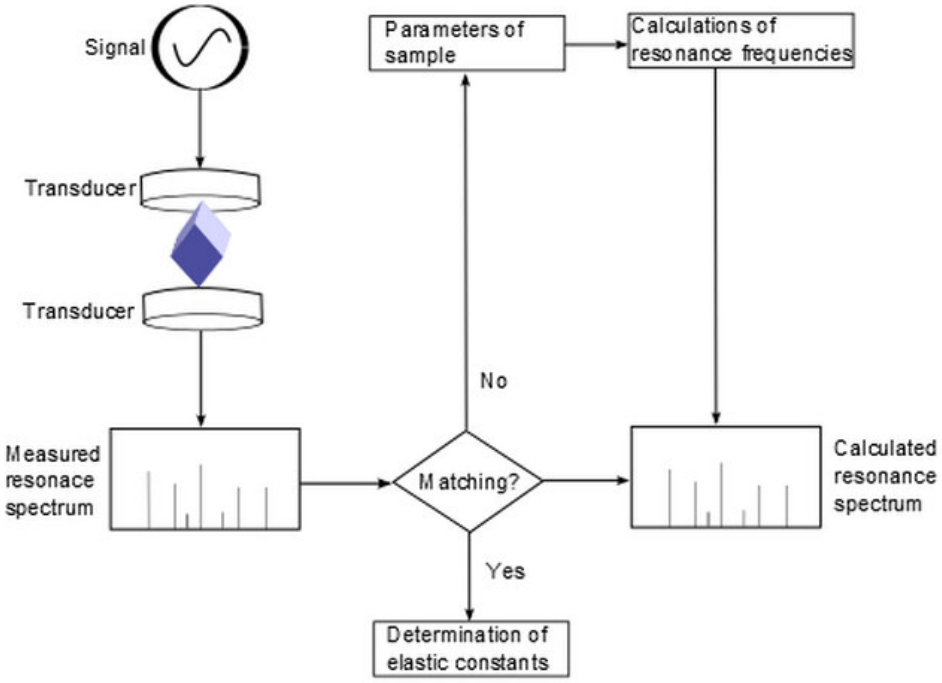

Figure 3.4: Schematic diagram of the RUS measurement and the fitting procedure of the elastic moduli. It is inspired by [20].

Figure3.4 illustrates the procedure of a RUS measurement. The sample is put between two transducers. The upper transducer is used to generate propagating waves with various frequencies. The second one is used as a detector to detect the transmitted waves, affected by resonance effects. The transmission is recorded and thus a spectrum with amplitude as a function of frequency is obtained. The resonance frequencies are then fitted with Lorentzian functions and their peak positions are extracted with the program "RUSdataReducer" (see appendix A1). The extracted resonance frequencies, g_i, are used in a fitting processes in order to adjust the elastic moduli of the measured sample. The application of this fitting process to a sample with rectangular parallelepiped shape was reported by I. Ohno [21] and the corresponding software is called "rectangular parallelepiped resonance (RPR)" (download from [22]).

In this fitting process, the dimensions of the sample and guessed elastic moduli have to be introduced as input parameters (see appendix A2). The guessed elastic moduli must be very close to the solution otherwise the software is not able to calculate reasonable values. In this manuscript, the initial elastic moduli were taken from already existing data of the x=4 compound, which will be published soon. The dimensions can be directly measured and are thus accurately enough.

From the initial parameters, the RPR code calculates theoretical resonance frequencies, f_i, from the energy equation according of the system. This procedure is pointed out in detail in reference [3].

The measured and calculated resonances are compared and a deviation, F, is calculated according to the Levenberg–Marquardt algorithm [3] with:

$$\mathrm{F} = \sum_{i=1}^{N} w_i (f_i - g_i)^2$$

Where, N is sum number of measured frequencies and w_i is a weight factor. The algorithm try to reduce F by changing the initial guessed elastic moduli and dimensions. The best obtained results of the dimensions, elastic moduli, resonance frequencies and the corresponding error are in a “rusout.dat” file (see appendix A4).

Data processing

Since some peaks are too small or overlapping with other peaks in the spectra, they cannot be extracted. These peaks must be introduced to the analysis by adding zero lines in the input file [3]. This procedure is necessary for the fitting procedure, since the order of the frequencies determine their relative contribution to certain elastic moduli and thus the resulting magnitude of these moduli (see appendix A3). Consequently, this step is repeated until the fitting procedure returns a reasonable agreement between the measured resonances and the resulting adjustment, indicated by a low deviation F. In the performed data analysis (see section 6.1) usually about 4 resonances are artificially introduced, depending on the quality of the spectrum.

4. Sample Descriptions

4.1 The system $Mn_{5-x}Fe_xSi_3$

The compounds in the series $Mn_{5-x}Fe_xSi_3$ crystallize hexagonal in the space group $P6_3/mcm$, as reported by Binczycka in 1973 [23]. The unit cell of one individual representative is shown in Figure 4.1. For the different stoichiometries, the Wyckoff positions [24] 4d and 6g are occupied in a disordered way by Mn and Fe with different probabilities. For example, in $MnFe_4Si_3$ the 4d position is occupied by 99.2% Fe and 0.8% Mn and the 6g position is occupied by 67.2% Fe and 32.8% Mn. The silicon atoms are incorporated into Wyckoff position 6g. The lattice parameters of the unit cell and volume decrease with increasing x due to the smaller atomic radius of the Fe-atom when compared to Mn [25].

The magnetic behavior of the compounds in the system $Mn_{5-x}Fe_xSi_3$ was investigated by Songlin et. Al. [2], leading to the magnetic phase diagram shown in Figure 4.2. It can be seen that different stoichiometries imply different magnetic ordering temperatures and that, in general, the magnetic transition temperatures increase with increasing Fe-concentration. The individual compounds of the series exhibit antiferromagnetic order for stoichometries with $x \leq 3$ and ferromagnetic order for the stoichometries with $x \geq 4$. For stochiometries with $3<x<4$ the antiferromagentic and ferromagnetic order co-exist.

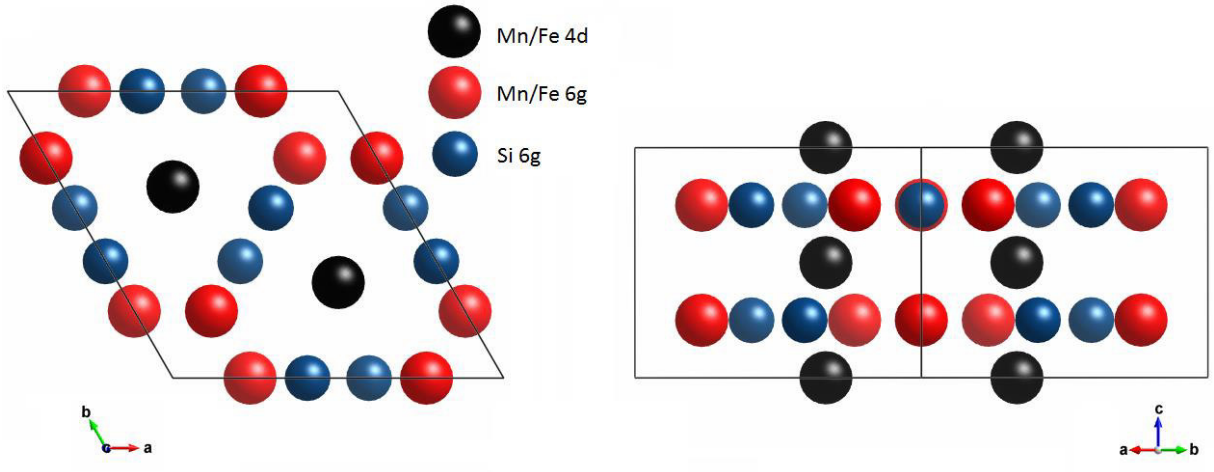

Figure 4.1: Schematic representation of the unit cell of individual compounds in the series $Mn_{5-x}Fe_xSi_3$ (left) projection along [001] and (right) projection along [110].

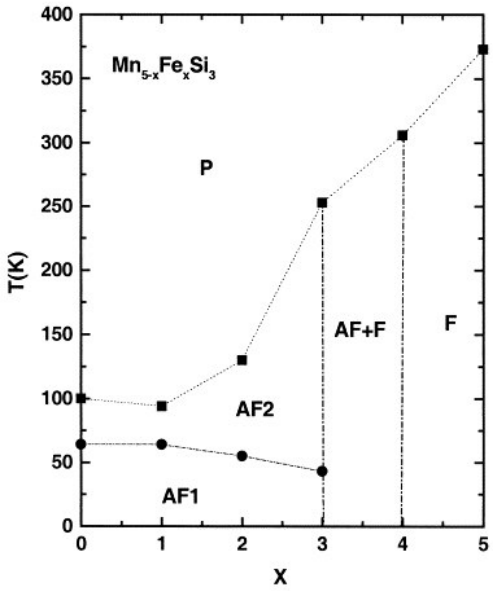

Figure 4.2: Magnetic phase diagram for the individual compounds in the series $Mn_{5-x}Fe_xSi_3$ (P=paramagnetic, AF=antiferromagnetic, F=ferromagnetic) [2].

4.2 Sample preparation

Polycrystalline samples of the individuals compounds in the series $Mn_{5-x}Fe_xSi_3$ with x=1 and 4 were prepared by induction melting [26] of stoichiometric amounts of Mn, Fe and Si. Approximately 80 g of the polycrystalline material were used for the growth of single crystals. The single crystals were prepared with the Czochralski method (see section 3.1) using a pulling rate of 15mm/h and tungsten as seed. The obtained ingots of $MnFe_4Si_3$ and Mn_4FeSi_3 are shown in Figure 4.3 a) and Figure 4.3 b), respectively. In the case of Mn_4FeSi_3, the ingot broke during the growth, probably related to a strong temperature gradient in the sample. However, the individual parts were still useable for the subsequent measurements.


a)


b)

Figure 4.3: a) The cylindrical ingot of $MnFe_4Si_3$. b) The broken ingot of Mn_4FeSi_3.

After the synthesis, the orientations and the quality of the crystals were checked with the Laue method (see section 3.2). The Laue diffraction diagrams of the crystals aligned along the [001]-axis are displayed in Figure 4.4. In the diffraction diagrams the six fold symmetry is clearly visible. The crystals were moved into different orientations and the resulting diffraction patterns were inspected. This confirmed that both crystals were composed of one individual single crystal.

Afterwards, the obtained single crystals needed to be cut to rectangular parallelepiped with Traveling EDM (see section 3.3) to obtain suitable specimen for the RUS measurements. For these crystals were first cut parallel to the c-axis and then a second cut parallel to the a (or b)-axis was performed. The third cut was chosen perpendicular to the other two cuts. Consequently, the faces of the cut crystal exhibit 90° angles between each other. Since, the unit cell is hexagonal and the angle between a-axis and b-axis is 120°, the axes are a (or b), 1/2a +b (or 1/2b + a) and c for the cut parallelepiped shape.

Both samples were polished after cutting in order to obtain even surfaces without cracks. This is necessary as cracks can result in geometrical errors and reduce the accuracy of the subsequent RUS measurements. The $MnFe_4Si_3$ sample with a size of 1.38mm x 2.22mm x 1.404mm and the Mn_4FeSi_3 sample with a size of 0.925mm x 1.581mm x3.300mm are shown in Figure 4.5. The dimensions of the samples were measured with a digital micrometer, which has an accuracy of $\pm$0.01mm.

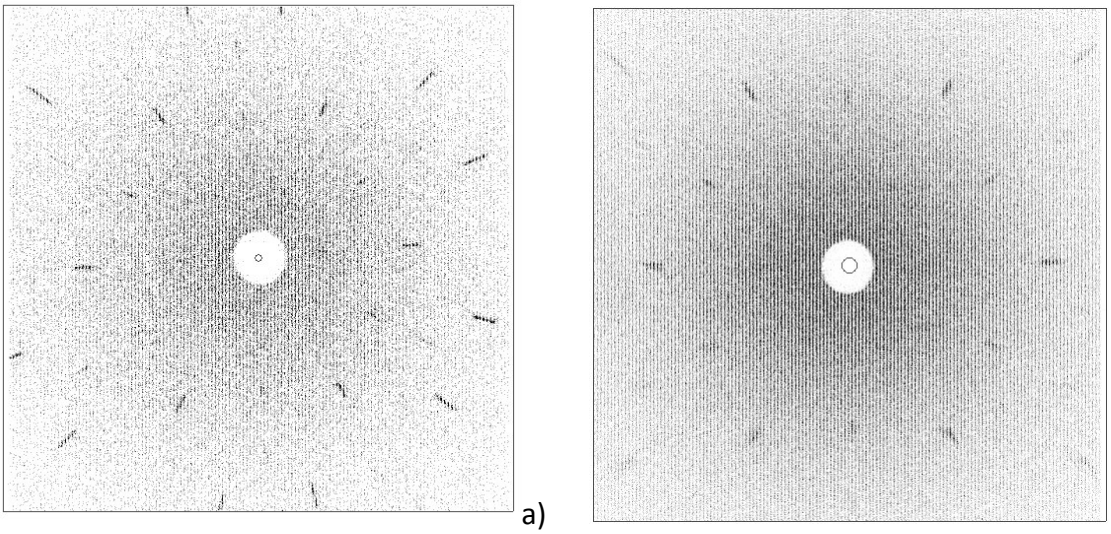

a) b)

Figure 4.4: The Laue diffraction diagram of a) $MnFe_4Si_3$ and b) Mn_4FeSi_3 along the [001]-direction.

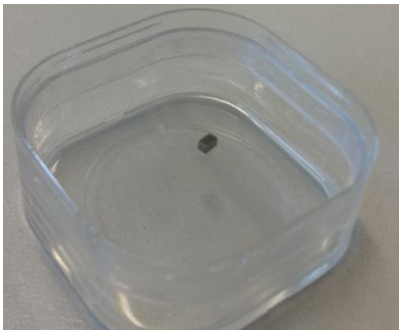
a)
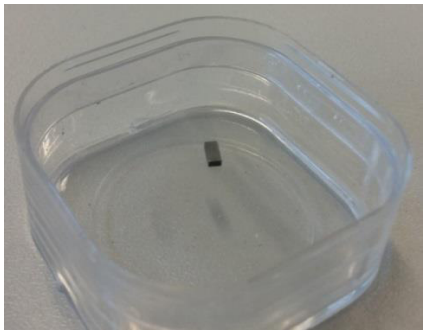
b)

Figure 4.5: The a) $MnFe_4Si_3$ and b) Mn_4FeSi_3 samples as cut for the RUS measurements.

5. Experimental

The RUS data is recorded with a low-temperature setup introduced as a probe into a Physical Properties Measurement System (PPMS). This instrument can change the temperature and magnetic field in the range from 1.8-400 K and ±8 T, respectively. The PPMS is shown in Figure 5.1 a), the RUS probe is shown in Figure 5.1 b). The sample is put between the two piezoelectric transducers, which are mounted to the probe, as shown in Figure 5.1 c).

a)

b)

c)

Figure 5.1: Photos of low-temperature setup for the RUS measurements. a) The Physical Properties Measurement System. b) The probe option for the RUS measurement. c) Mounting of the sample between the two transducers.

Before every measurement with this system, two kinds of reference measurements are performed. The first measurement is the recording of the background frequencies from the setup itself. This is done by measuring the empty probe. The obtained resonances are excluded for further analysis in the obtained data sets.

The second reference measurement is performed at room temperature with a simplified setup shown in Figure 5.2. This setup leads usually to better defined resonance frequencies with less noise due to the simpler mounting of the sample. Extracting and analyzing data of the room-temperature measurement can help to analyze the data obtained with the setup for low-temperature setup, because the modes are basically the same for the same sample.

Figure 5.2: The setup for RUS measurements at room temperature.

After the reference measurements, the sample is sandwiched between the two transducers of the probe. Then, the probe is inserted into the PPMS. Due to the weak coupling between sample and transducers and the tiny stages of the two transducers, the sample can shift or tilt when the probe is inserted. As a result, the transducer can lose the responding signal. This is checked with a test measurement. In case the sample is lost, the probe is taken out and the mounting process is repeated until a good test spectrum is obtained. After the test measurement, the sample can be measured at various temperatures or in various magnetic fields. The resonance frequencies are scanned by a connected frequency generator in combination with a computer.

6. Results and Discussion

6.1 Results

6.1.1 Investigation of intrinsic error

The $MnFe_4Si_3$ and Mn_4FeSi_3 sample were measured at room temperature with low-temperature and room-temperature setup along different axes in the absence of a magnetic field. The elastic moduli should be equal, since they depend only on the material and the sample shape. The observed differences can be understood as errors due to mounting the sample and deviations in the setup. For example, the sandwiched sample can tilt under the pressure of the upper transducer or the resulting force due to the mounting in the setup can be different. Especially the mounting in the low-temperature setup is difficult and thus larger errors are expected.

The Table 6.1 shows the extracted elastic moduli of the $MnFe_4Si_3$ sample. A comparison of the elastic moduli obtained from measurements with room-temperature and low-temperature setup reveals that the differences between the c_{11}, c_{33}, c_{12} c_{44} and c_{66} moduli are smaller than 0.4%. The c_{23} moduli exhibit differences about 1.5%. The obtained elastic moduli from measurements along different axis exhibit differences smaller than 0.3% in the c_{11}, c_{33}, c_{44}, and c_{66} moduli and about 1.1% in the c_{23} and c_{12} moduli.

Table 6.1: The obtained elastic moduli of $MnFe_4Si_3$ with errors measured with low-temperature (LT) setup and room-temperature (RT) setup. The unit of elastic modulus is GPa.

Setup	Axis	c_{11} ,c_{22}	c_{33}	c_{23} ,c_{13}	c_{12}	c_{44} ,c_{55}	c_{66}
LT- setup	Perpendicular to c-axis	241.5(7)	306(2)	61.6(9)	85.0(9)	70.8(2)	78.3(2)
RT- setup	Perpendicular to c-axis	241.91(9)	304.8(6)	61.0(1)	85.237(2)	70.927(7)	78.33(4)
	Perpendicular to c-axis	242.2(4)	305.41(6)	61.3(2)	85.8(6)	71.01(8)	78.19(8)
	c-axis	241.6(2)	305.2(2)	60.6(5)	84.9(3)	70.919(2)	78.3(1)

The Table 6.2 depicts the obtained elastic moduli of the Mn_4FeSi_3 sample. The elastic moduli obtained from measurements with room-temperature and low-temperature setup exhibit differences smaller than 0.6 % between the c_{11}, c_{33}, c_{44} and c_{66} moduli. The c_{12} moduli exhibit differences about 0.9 % and the c_{23} modulus exhibit a difference of 2.3 %. The obtained elastic moduli from measurements along different axis exhibit differences smaller than 0.4% in the c_{11}, c_{12}, c_{44}, and c_{66} moduli and about 1.0% in the c_{33} and c_{23} moduli.

Table 6.2: The obtained elastic moduli of Mn_4FeSi_3 measured with low-temperature (LT) setup and room-temperature (RT) setup. The unit of the elastic moduli is GPa.

Setup	Axis	c_{11}, c_{22}	c_{33}	c_{23}, c_{13}	c_{12}	c_{44}, c_{55}	c_{66}
LT- setup	c-axis	212(1)	268(3)	52(1)	97(1)	68.06(8)	57.7(2)
RT- setup	c-axis	212.4(1)	267(1)	51.7(2)	96.54(5)	68.034(1)	57.92(8)
	Perpendicular to c-axis	211.7(5)	270(2)	52.0(1)	96.2(4)	68.06(3)	57.75(9)
	Perpendicular to c-axis	212.30(3)	267(1)	51.3(6)	96.5(1)	67.98(6)	57.92(8)

The errors of the elastic moduli of all these measurements are, according to the output of the RPR code, smaller than 10 %. This value represents the error of the absolute value of the elastic moduli, strongly influenced by the sample shape and the model which was assumed for the analysis of the data. However, this value gives no indication for the relative error between different measurements with the same sample and the same applied model.

Comparing the obtained elastic moduli from measurements with different setups and along different axes, all differences in the moduli were found to be smaller than or near 1% for $MnFe_4Si_3$ and Mn_4FeSi_3, except the c_{23} modulus. Consequently, an error of 1% can be expected as the worst case scenario by re-mounting the sample. Nevertheless, in the following measurements with the low-temperature setup, the samples were measured without re-mounting in between the measurements. Thus, the relative error between the measurements without remounting will be probably much less than 1%. That indicates an observed tendencies of the elastic moduli, measured with changing magnetic field or temperature, are often reasonable, even if their absolute value changes by less than 1%.

Consequently, the obtained errors of the elastic moduli in this section are used as error bars in the following analysis.

6.1.2 RUS on $MnFe_4Si_3$ with low-temperature setup

The $MnFe_4Si_3$ single crystal was measured with applied magnetic fields in the range from 0 T to 0.5 T at room temperature. The field was applied perpendicular to the c-axis. The measured frequency range was 600 KHz to 4000 KHz.

A representative resonance spectrum of $MnFe_4Si_3$ at room temperature in the absence of magnetic field is shown in Figure 6.1. The depicted y-axis of the resonance spectrum is the square of the real and imaginary components of the lock-in amplifier signal.

The application of a magnetic field changes the elastic moduli in a material. Consequently, the resonance frequencies also change if a magnetic field is applied, as shown in Figure 6.2. The magnetic field dependence of selected resonance frequencies is shown in Figure 6.3. The resonance frequencies increase with increasing magnetic field. As the elastic moduli are intimately related to these resonances, this indicates that the stiffness of the material becomes larger with applied magnetic field.

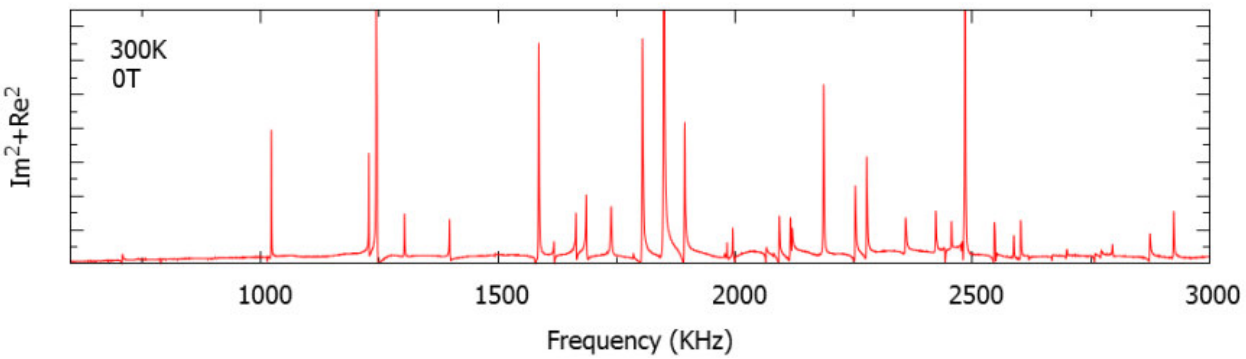

Figure 6.1: Resonance spectrum of $MnFe_4Si_3$ at room temperature in 0 T.

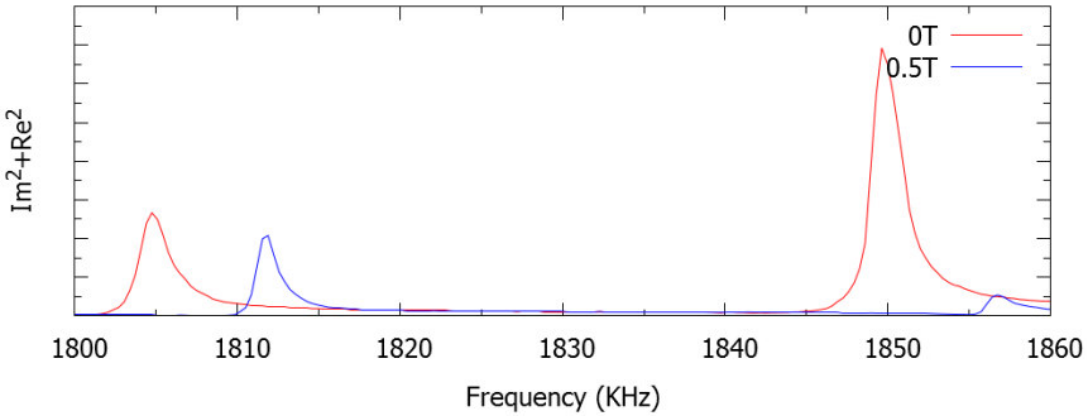

Figure 6.2: Section of the resonance spectra of $MnFe_4Si_3$ at room temperature with 0 T and 0.5 T. The applied magnetic field leads to a change of the resonance frequencies.

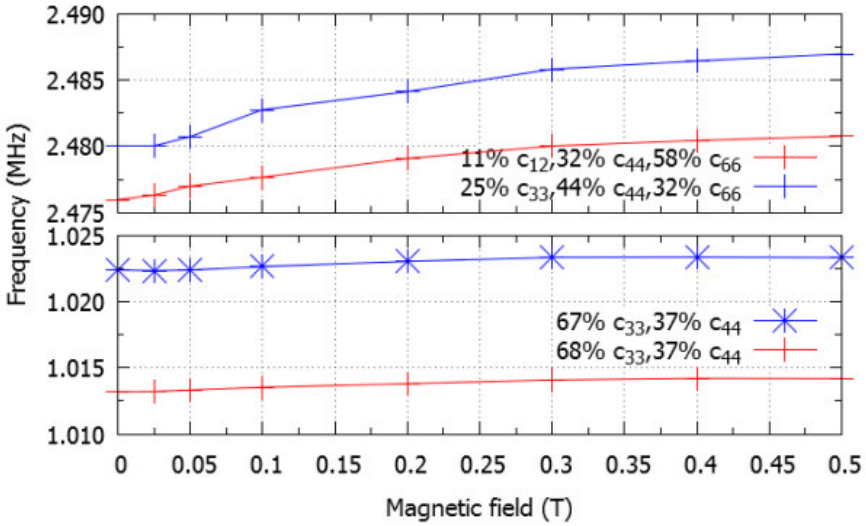

Figure 6.3: Four selected resonance frequencies as a function of magnetic field. All four resonance frequencies increase with increasing magnetic field.

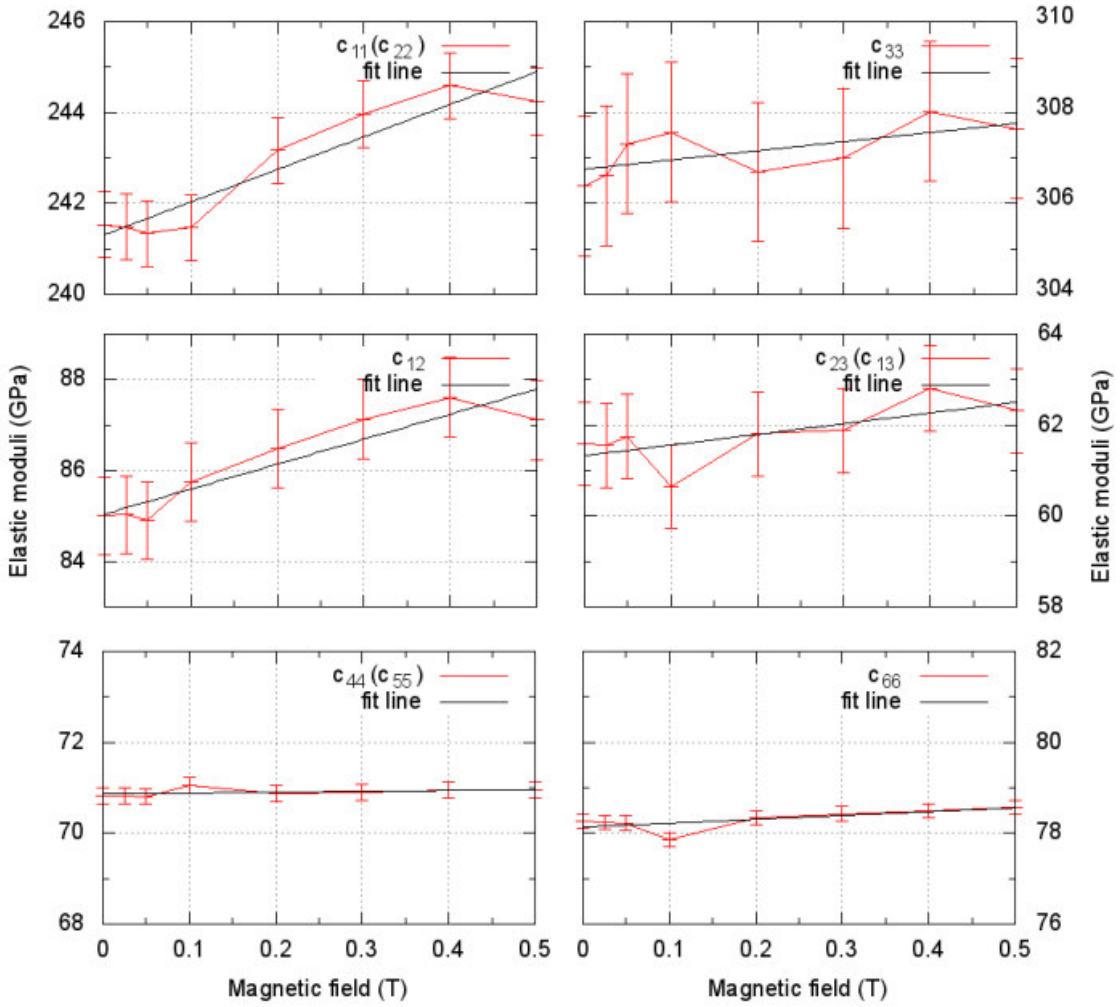

Figure 6.4: The elastic moduli of $MnFe_4Si_3$ at room temperature with a linear fit to the data. The given error bar is the relative error calculated in section 6.1.1.

Table 6.3: The slope, *m*, of the linear fit in Figure 6.4 indicates the change of the elastic moduli. The slope *m* is in units of GPa/T.

Elastic moduli	c_{11},c_{22}	c_{33}	c_{23},c_{13}	c_{12}	c_{44},c_{55}	c_{66}
m	7(1)	2(1)	2(1)	5.4(9)	0.2(2)	0.8(3)

The obtained elastic moduli of the $MnFe_4Si_3$ sample, calculated from the extracted resonance frequencies, with the linear fit are shown in Figure 6.4. The obtained slope *m* of the linear fit is given in Table 6.3. The c_{11} and c_{12} elastic moduli increase most drastically with increasing magnetic field. The c_{33} and c_{23} elastic moduli slightly increase with increasing magnetic field, but in the limits of the error bar. On the other hand, the c_{44} and c_{66} elastic moduli (which is calculated according to $\frac{c_{11}-c_{12}}{2}$) stay basically constant as a function of magnetic field.

6.1.3 RUS on Mn_4FeSi_3 with low-temperature setup

The Mn_4FeSi_3 single crystal was measured along the c-axis in a temperature range from 20 K to 300 K without magnetic field. In addition, the crystal was measured at 65 K with magnetic fields in the range of 0 T and 0.5 T and the field was applied parallel to the c-axis. The chosen frequency range was from 100 KHz to 4000 KHz.

The extraction of the elastic moduli was only possible in the range of 150 K and 300 K. The spectra below 150 K exhibited a high level of noise and the resonance peaks could not be extracted accurately. This effect is probably due to the piezoelectric transducers, which become harder and less sensitive with lower temperatures. Still, a limited number of resonance frequencies in the low frequency region could be extracted to lower temperatures.

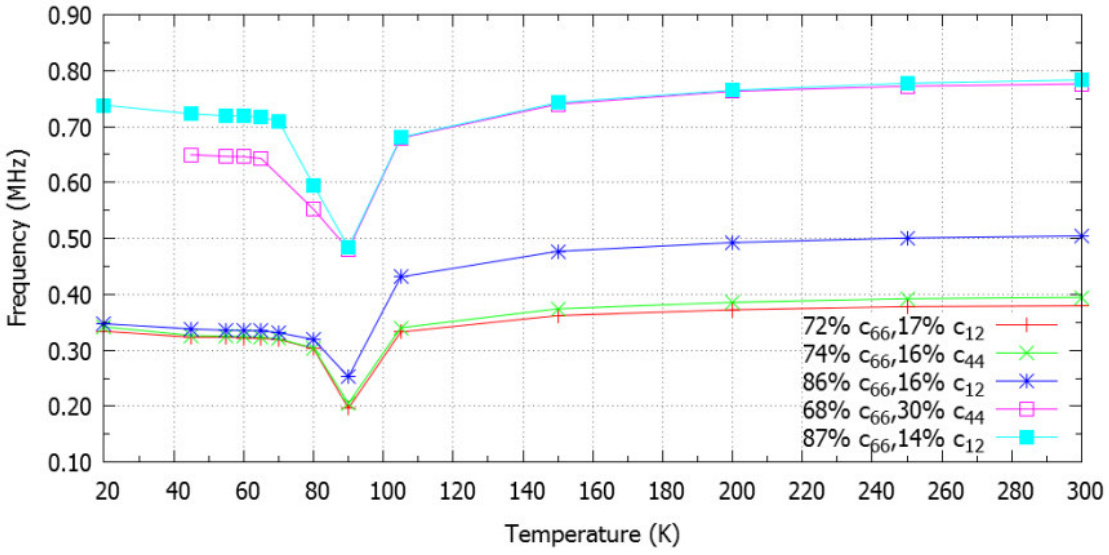

Figure 6.5: Five selected resonance frequencies as a function of temperature.

Figure 6.5 depicts five selected resonance frequencies as a function of temperature between 20 K and 300 K. The resonance frequencies decrease continuously with decreasing temperature in the range from 300 K to 105 K. At about 90 K a drop occurs in the resonance frequencies. This anomaly arises from a magnetic transition, which occurs about 90 K [2]. Below 90 K the frequencies rise again and the resonance frequencies start to combine or to split, respectively, indicating a strong change in the elasticity. In the literature [2], a second magnetic transition around 65 K is reported, however, no indication of a change of the resonance spectra as a result of this transition can be found.

A section of the measurements on Mn_4FeSi_3 under applied magnetic field at 65 K are depicted in Figure 6.6. Due to the low temperature and, as a consequence of this, the high level of noise, only a few selected resonance frequencies could be reliably extracted. The resonance frequencies at 0.320 MHz and 0.328 MHz decrease with rising magnetic field. This indicates a lower stiffness of the corresponding elastic moduli at low frequencies. The resonance frequency at 0.322 MHz seems to be independent of the applied magnetic field.

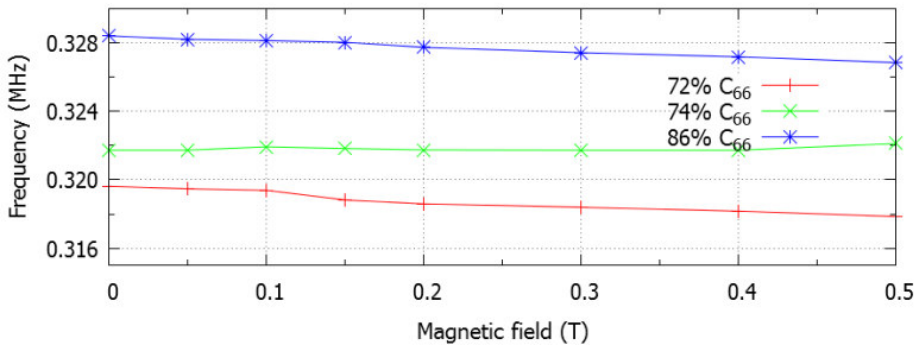

Figure 6.6: Three resonance frequencies extracted from the measurements with applied magnetic field on Mn_4FeSi_3 at 65 K.

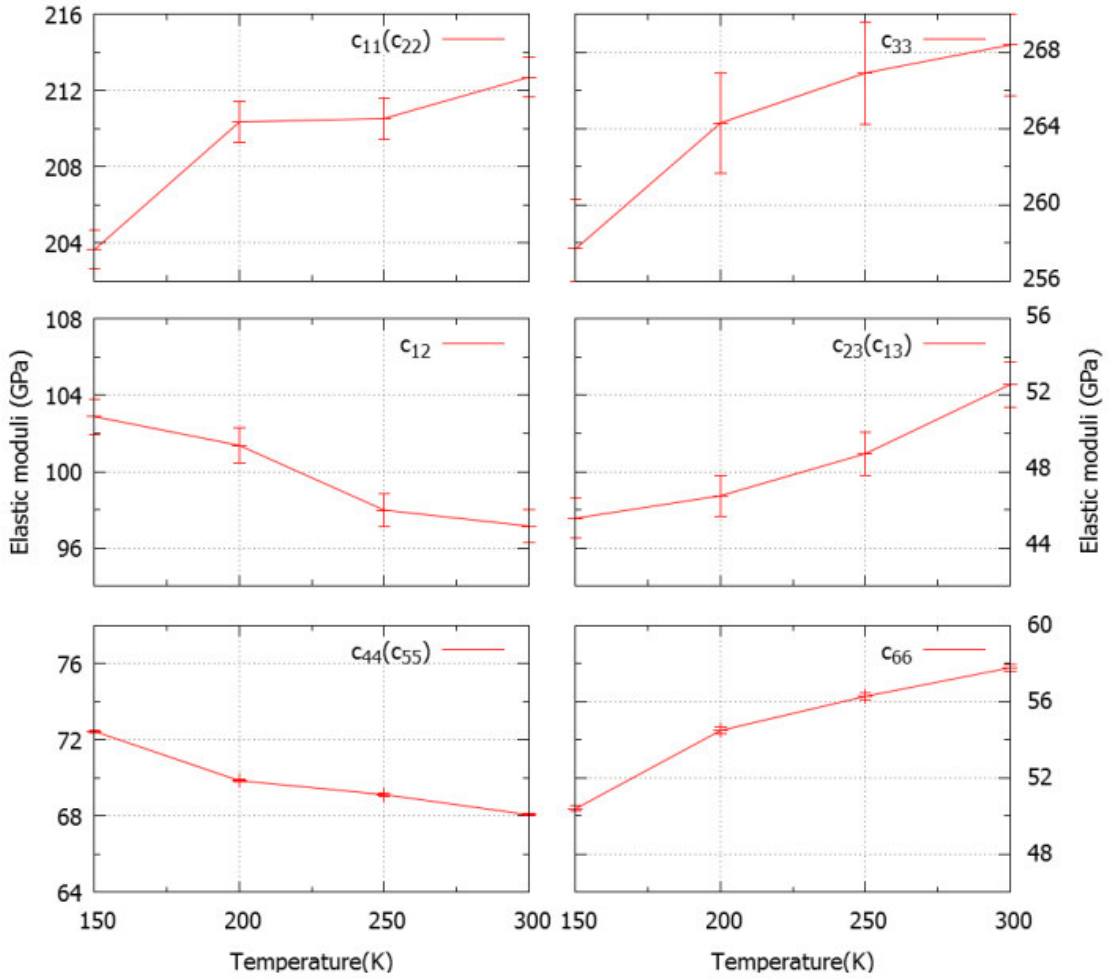

Figure 6.7: The elastic moduli of Mn_4FeSi_3 as a function of temperature in the absence of magnetic field. The given error bar is the relative error calculated in section 6.1.1.

The temperature dependence of the elastic moduli of the Mn_4FeSi_3 sample in the absence of magnetic field, calculated from the extracted resonance frequencies, are shown in Figure 6.7. It can be clearly seen the elastic moduli change significantly with decreasing temperature. The c_{11}, c_{33}, c_{23} and c_{66} elastic moduli decrease with decreasing temperature, while the c_{12} and c_{44} elastic moduli increase with decreasing temperature.

6.2 Discussion

The two single crystals $MnFe_4Si_3$ and Mn_4FeSi_3 were investigated with RUS, in order to quantify the elastic moduli by measuring their resonance frequencies. The $MnFe_4Si_3$ sample was measured in various magnetic fields between 0 T and 0.5 T at room temperature. The Mn_4FeSi_3 sample was measured at different temperature between 20 K and 300 K without magnetic field and under various applied magnetic fields between 0 T and 0.5 T at 65 K.

In the literature it is reported that about 300 K the $MnFe_4Si_3$ material exhibits a transition from paramagnetic order to ferromagnetic order [2]. At this temperature, in the transition region, the elastic moduli of $MnFe_4Si_3$ were recorded. It was found that the elastic moduli c_{11}, c_{33}, c_{12} and c_{23} become larger and the shear moduli c_{44} and c_{66} stay nearly constant. This behavior indicates that $MnFe_4Si_3$ material becomes harder under applied magnetic fields. The reason for this observation could be magnetostriction, leading to a decrease of the sample volume and thus an increase of the elastic moduli. The overall change of the elastic moduli with an applied 0.5 T is only about 1%.

The extracted elastic moduli of the Mn_4FeSi_3 sample indicate that the material becomes harder along the elastic moduli c_{11}, c_{33}, c_{23} and c_{66} with increasing temperature. In contrast, the c_{12} and c_{44} elastic moduli decrease with an increase in temperature. Commonly, temperature increase leads to positive thermal expansion and thus to a decrease of the stiffness. But, in our results, the opposite behavior of some elastic moduli in Mn_4FeSi_3 was found.

According to the data reported by Songlin et. Al. [2], the compound Mn_4FeSi_3 has two magnetic transitions at 94 K and 64.5 K, respectively. The investigation of the single crystalline sample of Mn_4FeSi_3 revealed an anomalous behavior of the resonance frequencies at approximately 90 K, which might well be related to the magnetic transition at 94 K where to compound changes from paramagnetic to anti-ferromagnetic order. The magnetic transition might be accompanied by changes in the unit cell volume and consequently changes in the stiffness of the sample. On further decreasing of the temperature to 65 K, no indication reflecting the second magnetic transition was found in the resonance spectra. The second magnetic transition is related to a change from a collinear antiferromagnetic phase to a non-collinear antiferromagnetic phase [2] and

probably, there is no influence from this type of transition on the elasticity of the compound or the changes are too small to be observed at this low temperature where the level of noise in the measurement is considerable.

The measurements on Mn_4FeSi_3 at 65 K in an applied magnetic field indicate that the applied magnetic field has only a small influence on the resonance frequencies. The corresponding moduli become slightly softer as a response to the magnetic field.

The obtained elastic moduli of $MnFe_4Si_3$ and Mn_4FeSi_3 at room temperature without an applied magnetic field are shown in Table 6.4. The indicated errors are taken directly from the RPR code and are thus the absolute errors of the measurements. The relative errors calculated in section 6.1.1 cannot be used, since the samples are different. The absolute errors bars of the results overlap, but the elastic moduli represent a trend such as the most $MnFe_4Si_3$ moduli are larger than the Mn_4FeSi_3 moduli. The lattice parameters of Mn_4FeSi_3 and $MnFe_4Si_3$ were investigated by Vancliff Johnson [25] and are shown in Table 6.5. The volume of the $MnFe_4Si_3$ unit cell is smaller than the volume of the Mn_4FeSi_3 unit cell in accordance with the smaller atomic radius of Fe when compared to Mn. The smaller volume can explain that the sample of $MnFe_4Si_3$ is harder, as the crystal structure is same and thus the atomic bonds within the structure will be similar.

Also the fact that the magnetic states of both compounds at room temperature are different, as Mn_4FeSi_3 is in a paramagnetic state while $MnFe_4Si_3$ is ferromagnetically ordered at room temperature [2], can have an influence the stiffness of the samples.

Table 6.4: Comparison of the elastic moduli of Mn_4FeSi_3 and $MnFe_4Si_3$. The units of elastic moduli are GPa.

	Axis	c_{11},c_{22}	c_{33}	c_{23},c_{13}	c_{12}	c_{44},c_{55}	c_{66}
Mn_4FeSi_3	c- axis	212(19)	268(25)	53(5)	97(9)	68(6)	58(5)
$MnFe_4Si_3$	Perpendicular to c-axis	241(19)	306(24)	61(5)	84(7)	71(5)	78(6)

Table 6.5: Lattice parameter and unit cell volume of Mn_4FeSi_3 and $MnFe_4Si_3$ at room temperature (data from reference [25]).

	a(Å)	*c*(Å)	*V*(Å^3)
Mn_4FeSi_3	6.8840	4.7876	196.5
$MnFe_4Si_3$	6.8004	4.7298	189.4

7. Summary

The investigated compounds $MnFe_4Si_3$ and Mn_4FeSi_3 are magnetocaloric materials with only a moderate MCE [2]. However, the advantage of these materials compared to other magnetocaloric materials is that they can be produced as single crystals, giving access to various measurement methods with larger information yield as compared to polycrystalline samples, *e.g.*, in case of Resonant Ultrasound Spectroscopy (RUS).

The $MnFe_4Si_3$ and Mn_4FeSi_3 single crystals were produced with the Czochralski method and investigated with RUS at different temperatures and various fields.

The results obtained on the $MnFe_4Si_3$ sample reveal that the elastic moduli c_{11}, c_{33}, c_{12} and c_{23} become larger and the shear moduli c_{44} and c_{66} stay nearly constant with increasing magnetic field. This indicates that the sample becomes on average harder. One possible explanation could be magnetostriction which accompanies the onset of ferromagnetic order and leads to a decrease of the sample volume and thus to an increase of the elastic moduli.

The extracted elastic moduli of the Mn_4FeSi_3 sample in the range from 150 K to 300 K indicate that the material becomes harder along the elastic moduli c_{11}, c_{33}, c_{23} and c_{66} and softer along the c_{12} and c_{44} elastic moduli with increasing temperature. Below this temperature range, the resonance frequencies exhibit a strong anomaly at about 90 K. This temperature nearly coincides with the onset of antiferromagnetic ordering in this material [2] and the observed anomaly thus most probably reflects the magnetic transition. The second magnetic transition reported in the literature at 65 K [2], which corresponds to a transition from an anti-ferromagnetic to another anti-ferromagnetic state, is not reflected in the elastic moduli of the material.

By comparing the obtained elastic moduli of $MnFe_4Si_3$ and Mn_4FeSi_3 at room temperature, it is found that the former material is harder than the latter which corresponds well with the fact that the unit cell volume of $MnFe_4Si_3$ is smaller than the one of Mn_4FeSi_3 [25], and thus provides an explanation for the increased stiffness. However, also the fact that Mn_4FeSi_3 and $MnFe_4Si_3$ are not in the same magnetic state at room temperature [2], can have an influence over the stiffness of the materials.

References

[1] V.K Pecharsky K.A. Gschneidner, Jr. Int. J. Refrig., 31:945, 2008

[2] Songlin, Dagula, O. Tegus, E. Bruck, J. C. P. Klaasse, F. R. de Br, and K. H. J. Buschow. Journal of Alloys and Compounds, 334:249–252, 2002.

[3] Migliori, Albert and John L. Sarrao. Resonant Ultrasound Spectroscopy: applications to physics, materials measurements, and nondestructive evaluation, July 31 1997

[4] Pamela Burnley, Tensors: Stress, Strain and Elasticity, University of Nevada Las Vegas.

[5] L.D. Landau & E.M. Lifshitz Theory of Elasticity (Volume 7 of A Course of Theoretical Physics) Pergamon Press, 1970

[6] NDT source center, Sound Propagation in Elastic Materials, http://www.ndt-ed.org (15.9.14)

[7] Simple Harmonic Motion(SHM), http://www.physbot.co.uk (15.9.14)

[8] Burton, W.K. and Cabrera, N. "Crystal growth and surface structure. Part II" Discuss. Faraday Soc. 5, 40-48, 1949

[9] Pablo Cubillas and Michael W. Anderson Synthesis Mechanism: Crystal Growth and Nucleation

[10] Cristal_ou_amorphe.svg: Cdang Everything else: Sbyrnes321 - Cristal ou amorphe.svg Crystalline polycrystalline amorphous.svg

[11] Bragg's Law of Diffraction, The Electron Microscopy Site, http://www.microscopy.ethz.ch/bragg.htm (15.9.14)

[12] V. Franco, J.S. Blázquez, B. Ingale, and A. Conde. The Magnetocaloric Effect and Magnetic Refrigeration Near Room Temperature: Materials and Models. 2012

[13] K. H. J. Buschow R.R. de Boer O.Tegus, E. Brueck. *Lett. Nat*., 415:150, 2002

[14] J. Czochralski, A new method for the measurement of the crystallization rate of metals, Zeitschrift für Physikalische Chemie, 92 : 219–221, 1918

[15] B. D. Cullity, S. R. Stock. Elements of X-ray diffraction, 1956

[16] Laue method, University of Liverpool, http://www.matter.org.uk (15.9.14)

[17] MWL 100 Real-Time Back-Reflection Laue Camera System, Stanford University, http://www.stanford.edu. (15.9.14)

[18] Tech Briefs - EDM of Copper Beryllium, Materion, http://materion.com (15.9.14)

[19] Brian Zadler, Jerome H.L. Le Rousseau,JohnA.Scales & Martin L. Smith. Resonant ultrasound spectroscopy: Theory and application.

[20] Change in the elastic constants with thermal embrittlement of duplex stainless steel. Tetsu ICHITSUBO, Masakazu TANE, Hirotsugu OGI, and Masahiko HIRAO. Graduate School of Engineering Science, Osaka University, Osaka 560-8531

[21] I. Ohno, “Free vibration of a rectangular parallelepiped crystal and its application to determination of elastic constants of orthotropic crystal,” Journal of Physics of the Earth, vol. 24, pp. 355–379, 1976.

[22] Magnet Lab, University of Florida, http://www.magnet.fsu.edu/inhouseresearch/rus/

[23] Binczycka, Z. Dimitrijevic, B. Gajic, and A. Szytula. Atomic and magnetic structure of Mn5−xFexSi3.Physica Status Solidi (a), 19:K13–K17, 1973.

[24] Lev. Kantorovich. Quantum Theory of the Solid State: An Introduction, 2004

[25] Vancliff Johnson, J.F. Weiher, C.G. Frederick, D.B. Rogers Magnetic and Mössbauer effect studies of Mn_5Si_3:Fe_5Si_3 solid solutions, 1971

[26] Induction heating, http://www.richieburnett.co.uk (15.9.14)

Appendix

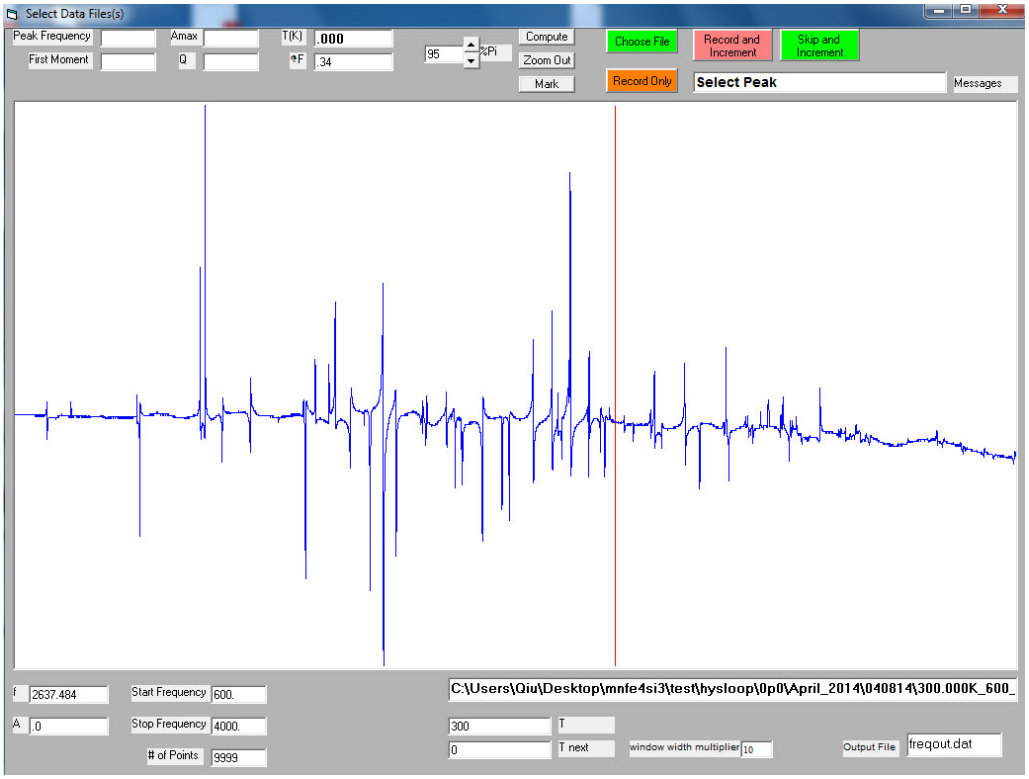

Figure A1: Common spectrum with resonance frequencies. The frequencies are extracted with the program "RUSdataReducer". The spectrum is recorded on $MnFe_4Si_3$ at room temperature in the absence of a magnetic field.

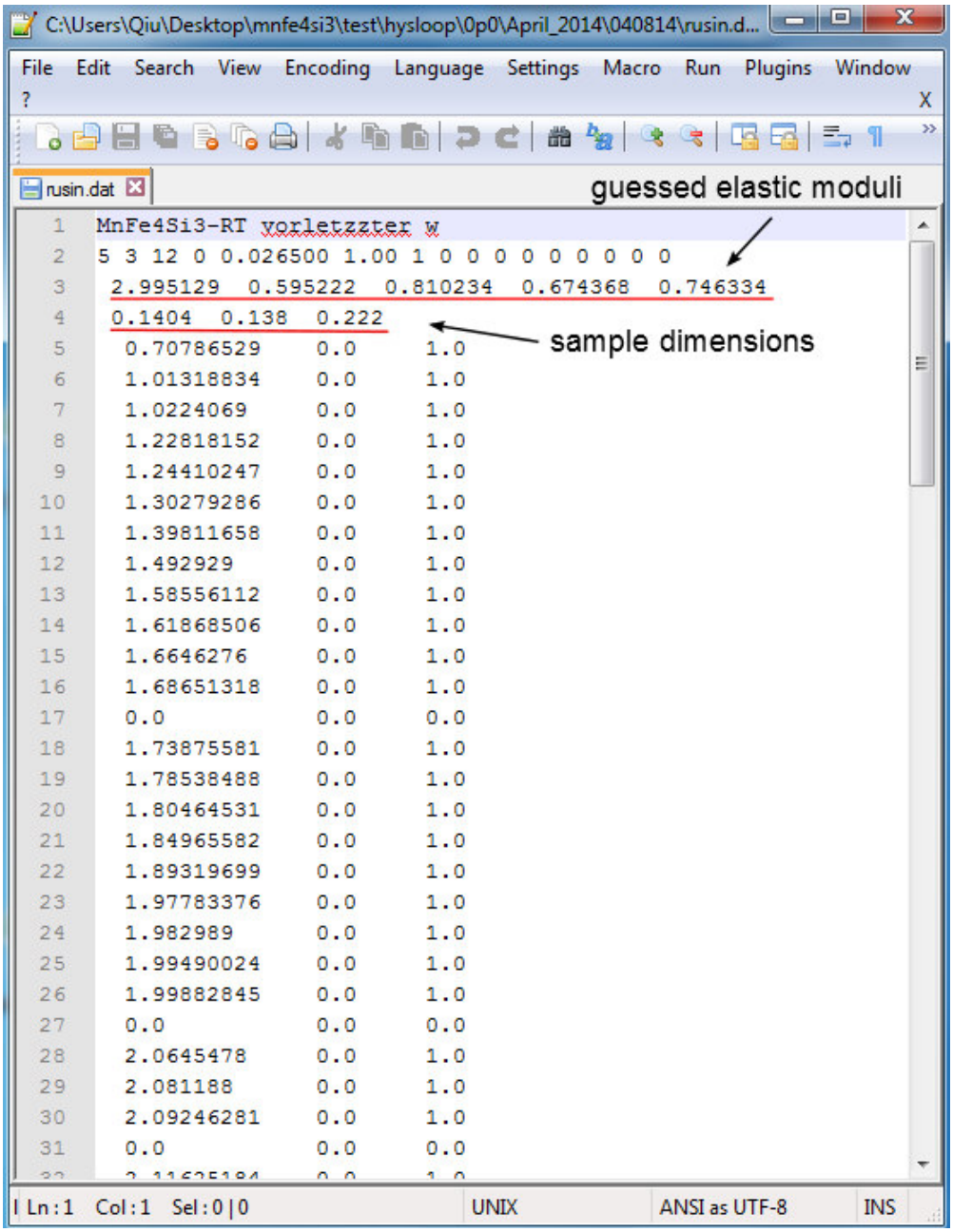


```
1  MnFe4Si3-RT vorletzzter w
2  5 3 12 0 0.026500 1.00 1 0 0 0 0 0 0 0 0 0
3   2.995129   0.595222   0.810234   0.674368   0.746334
4   0.1404   0.138   0.222
5    0.70786529     0.0      1.0
6    1.01318834     0.0      1.0
7    1.0224069      0.0      1.0
8    1.22818152     0.0      1.0
9    1.24410247     0.0      1.0
10   1.30279286     0.0      1.0
11   1.39811658     0.0      1.0
12   1.492929       0.0      1.0
13   1.58556112     0.0      1.0
14   1.61868506     0.0      1.0
15   1.6646276      0.0      1.0
16   1.68651318     0.0      1.0
17   0.0            0.0      0.0
18   1.73875581     0.0      1.0
19   1.78538488     0.0      1.0
20   1.80464531     0.0      1.0
21   1.84965582     0.0      1.0
22   1.89319699     0.0      1.0
23   1.97783376     0.0      1.0
24   1.982989       0.0      1.0
25   1.99490024     0.0      1.0
26   1.99882845     0.0      1.0
27   0.0            0.0      0.0
28   2.0645478      0.0      1.0
29   2.081188       0.0      1.0
30   2.09246281     0.0      1.0
31   0.0            0.0      0.0
```

Figure A2: The input file with recorded resonance frequencies and sample parameters. The data is recorded on $MnFe_4Si_3$ at room temperature in the absence of a magnetic field.

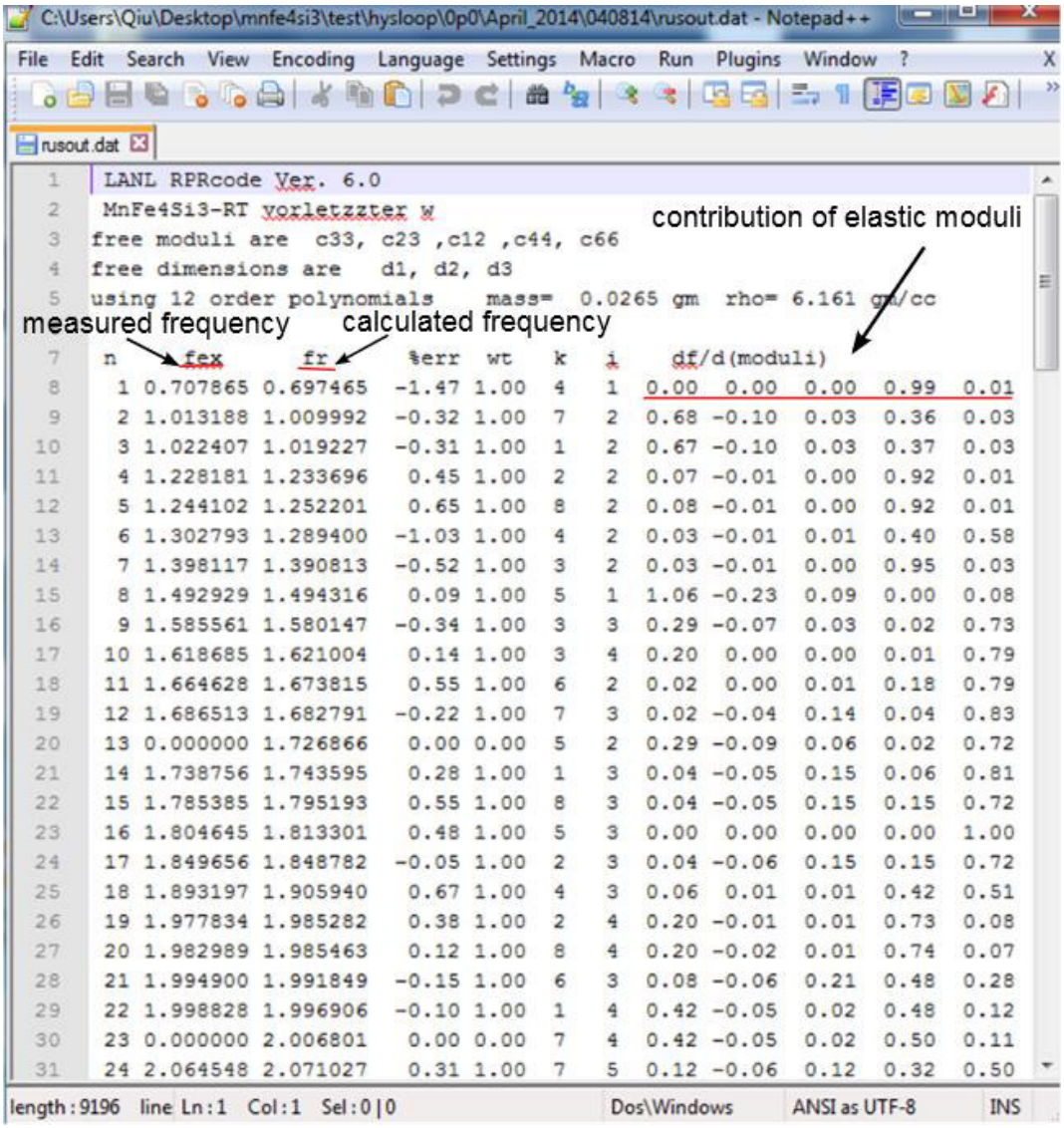

Figure A3: Top part of the RPR output. The measured and calculated resonance frequencies are given with their relative contribution to certain elastic moduli. The output file is recorded on $MnFe_4Si_3$ at room temperature in the absence of a magnetic field.

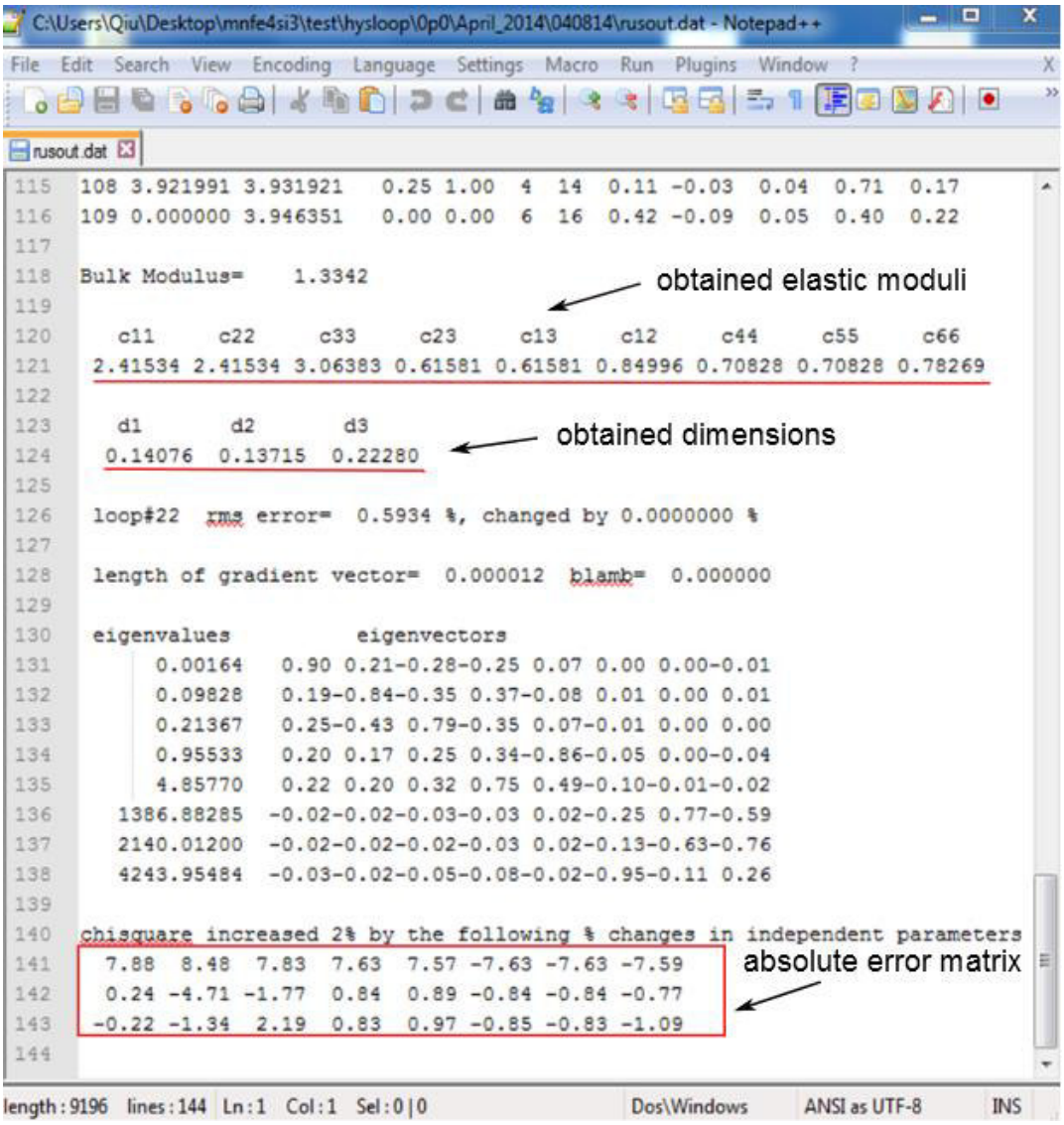

Figure A4: Bottom part of the RPR output file. The obtained elastic moduli, dimensions and the corresponding errors are listed.